Journal of Inorganic Biochemistry 197 (2019) 110696

Contents lists available at ScienceDirect

Journal of Inorganic Biochemistry

journal homepage: www.elsevier.com/locate/jinorgbio

Novel binuclear and trinuclear metal (II) complexes: DNA interactions and in vitro anticancer activity through apoptosis

Zhenxin Zhao, Junshuai Zhang, Shuangcheng Zhi, Wei Song, Jin'an Zhao*

College of Material and Chemical Engineering, Henan University of Urban Construction, Henan 467036, China

ARTICLE INFO

Keywords:
Metal (II) complexes
Reactive oxygen species
DNA interactions
In vitro anticancer activity

ABSTRACT

A water soluble trinuclear copper(II) complex and a binuclear cobalt(II) complex, namely $Cu_3(ppbm)_2(SO_4)_3$ (**1**) and $Co_2(ppbm)_2(NO_3)_4$ (**2**) (ppbm = 2-(pyridin-2-yl)-1-(pyridin-3-ylmethyl)- 1H-benzo[*d*]imidazole), have been successfully synthesized and characterized by elemental analysis, IR Spectroscopy, electrospray ionization mass spectra (ESI-MS). The interaction of the new complexes with DNA has been explored using spectroscopy methods, indicating that the complexes **1** and **2** bind to DNA via noncovalent interactions. DNA cleavage experiment suggested that the complex **1** exhibits efficient DNA cleavage activities in the presence of ascorbate (Asc), hydrogen peroxide may serve as the major cleavage active species. The cytotoxicity assay showed that complex **1** exhibited significant inhibitory activity toward the proliferation of several tumor cell lines, with a lower IC_{50} value than cisplatin and complex **2**, indicating that it had the potential to act as effective anticancer agent. The morphological staining assays showed that **1** apparently induced the TFK-1 cells apoptosis. Besides, cellular uptake experiment on TFK-1 cells revealed that complex **1** accumulates primarily inside the nucleus. The apoptosis was attributable to the metal-assisted generation of reactive oxygen species (ROS).

1. Introduction

The widespread success of cisplatin and related platinum-based drugs in the clinical treatment of various types of neoplasias has placed coordination chemistry of metal-based drugs in the frontline in the fight against cancer [1,2]. However, these platinum-based antitumor agents are associated with resistance, serious toxicity and other side effects during therapy processes, which severely limited its efficacy and applications in clinic [3,4]. To this end, alternative metal-based drug designs that are distinct from cisplatin and have different actions of mechanism at molecular level are being explored [5].

Currently, some inert metal complexes have been tested as anticancer agents [6–11]. Copper as a biologically relevant element, is involved in enzymatic functions and could selectively permeate the cancer cell membranes [12]. Its complexes have exhibited potent anticancer activity with low general toxicity [13,14,15], whose biodistribution, accumulation, and proliferation inhibition process seem to be different from those of platinum complexes [16], which provide an opportunity to circumvent the tumor resistance to conventional platinum drugs. Also, cobalt, even being heavy metal, has been reported to be utilized in several tumor treatment [17]. Especially cobalt chloride, has been found to lead to apoptosis by inducing reactive oxygen species (ROS) generation [18,19,20,21], and $CoCl_2$ comes to hypoxia mimicking mechanisms. Moreover, benzimidazole ligands complexed with diverse metals behave well in aspects of nuclease activities and cytotoxicity against tumor cells the planar, rigid and hydrophobic features [22]. In particular, benzimidazole derivative, such as (2-((quinolin-8-ylimino) methyl) pyridine), has been reported to possess a significant in vitro anticancer activities and markedly DNA cleavage, protein binding activities by coordinating with copper(II) [23].

With the exception of discovering new novel compounds structurally dissimilar to cisplatin, a recent strategy in the field of metal based anticancer drugs was proposed, which is designing some bimetallic or even multimetallic agents aiming to obtain biological and pharmacological features [12]. A trinuclear monofunctional platinum complex based on N,N,N′,N′,N″,N″-hexakis(2-pyridylmethyl)- 1,3,5-tris(aminomethyl) benzene performed higher cytotoxicity than cisplatin, which was also ascertained different from the scenario for cisplatin interaction with human serum albumin (HSA) [25]. Also, several multinuclear ntb-Cu(II) complexes exhibited a much stronger cytotoxicity than that of mononuclear Cu(II) complex (ntb = tris[(benzimidazol-2-yl)methyl] amine) [26].

Take these into account, two novel copper and cobalt-benzimidazole complexes were synthesized in this paper, hoping to obtain multinuclear complexes with improved potency and lowered side effects. Their structures have been characterized by several means. In vitro

* Corresponding author.
E-mail address: zjinan@zzu.edu.cn (J. Zhao).

https://doi.org/10.1016/j.jinorgbio.2019.110696
Received 25 October 2018; Received in revised form 20 April 2019; Accepted 22 April 2019
Available online 10 May 2019
0162-0134/

antiproliferative activity of $Cu_3(ppbm)_2(SO_4)_3$ (**1**) and $Co_2(ppbm)_2(NO_3)_4$ (**2**) (ppbm = 2-(pyridin-2-yl)-1-(pyridin-3-yl-methyl)- 1H-benzo[*d*]imidazole), was investigated against several cancer cell lines, the anticancer properties of the two complexes, which included cellular localization, cell death type determination, DNA interaction studies were explored using a variety of methods.

2. Experiment section

2.1. Materials and general methods

All reagents were commercially obtained and were used as received without further purification. Elemental analysis was carried out on a Flash EA 1112 elemental analyzer (Thermo Fisher Scientific, Waltham, MA, USA). Electrospray ionization mass spectra (ESI-MS) were measured on a Thermo Scientific LCQ fleet ESI-MS spectrometer. Infrared spectra with a KBr pellet were obtained using a Fourier transform infrared spectrometer (PerkinElmer, Waltham, MA, USA) in the region of 400–4000 cm^{-1}. Circular dichroism (CD) spectra were obtained on an MOS-500 instrument (Bio-Logic Science Instruments, Seyssinet-Pariset, France). Thermogravimetric experiments were performed on a Mettler Toledo TGA/SDTA instrument at a heating rate of 10 °C.min^{-1}.

2.2. Synthesis of $Cu_3(ppbm)_2(SO4)_3$ (1)

$CuSO_4{\cdot}5H_2O$ (0.09 mmol, 0.0231 g) were placed in a glass reactor (10 mL), after a full dissolution of 1 mL water, adding a solution of 1 mL acetonitrile. Subsequently, 1 mL of an ethanol solution of ppbm (0.02 mmol, 0.0057 g) was dropwise added into the glass reactor and the glass bottle with the mixed solution was heated at 85 °C for 60 h, then gradually cooled to room temperature at a rate of 5 °C·h^{-1}. Light blue diamond crystals were formed at the bottom of the glass reactor. The yield (based on Cu) was 59%. Elemental analysis (%) Calcd. For $C_{40}H_{51}Cu_3N_8O_{23}S_3$: C, 36.99; H, 3.96; N, 8.63; Found: C, 37.02; H, 3.94; N, 8.58. ESI-MS (MeOH) 525.29 $[M + H]^+$. IR (KBr/pellet, cm^{-1}): 3432 s, 2921 w, 2853 w, 1610 m, 1433 s, 1384 s, 1304 w, 738 w, 699 w.

2.3. Synthesis of $Co_2(ppbm)_2(NO_3)_4$ (2)

The synthesis procedure of complex **1** was similar to complex **2**, except that $Co(NO_3)_2$ (0.03 mmol, 0.0055 g) and ppbm (0.02 mmol, 0.0057 g) were used as the materials. Dark red rod crystals were generated at the bottom of the glass reactor. The yield (based on Co) was 75%. Elemental analysis (%) Calcd. for $C_{36}H_{28}Co_2N_{12}O_{12}$: C, 46.07, H, 3.01, N, 17.91. Found: C, 46.17, H, 3.06, N, 17.89. ESI-MS (MeOH) 912.83 $[M + H]^+$. IR (KBr/pellet, cm^{-1}): 3432 s, 2921 w, 2853 w, 1610 m, 1433 s, 1384 s, 1304 w, 738 w, 699 w.

2.4. Crystal structure determination

High-quality crystals of complexes **1** and **2** were collected from the parent liquid and mounted on a glass fiber. Single crystal X-ray diffraction data was obtained on a SuperNova system with graphite monochromated Cu-Kα radiation (λ = 1.54184 Å) at 100.01(10) K for complex **1** and 293(2) K for **2**, which was resolved and refined by using the OLEX2 crystallographic program **[27]**. Anisotropic thermal parameters were assigned to refine all non-hydrogen atoms. Based on observed reflections and variable parameters, the final cycle of full-matrix least-squares refinement was obtained. The contribution of disordered solvent in complex **1** was subtracted from the corresponding diffraction patterns by the squeeze procedure using PLATON software **[27,28]**. Crystallographic data such as crystal parameters and refinements for the two complexes are listed in Table 1, and the relevant bond lengths and angles are shown in Table 2.

Table 1
Crystallographic data and structural refinement for complexes **1** and **2**.

Complex	Complex 1	Complex 2
Formula	$C_{40}H_{51}Cu_3N_8O_{23}S_3$	$C_{36}H_{28}Co_2N_{12}O_{12}$
Formula weight	1298.69	938.56
Temp (K)	100.01(10)	293(2)
λ (Cu, Kα), Å	1.54184	1.54184
Crystal system	monoclinic	monoclinic
Space group	$P2_1$	I2/c
a (Å)	11.93033(16)	21.6480(11)
b (Å)	13.88055(14)	9.9748(6)
c (Å)	15.8166(2)	17.0871(9)
α(deg)	90	90
β(deg)	98.8222(12)	98.661(5)
γ(deg)	90	90
V ($Å^3$)	2588.24(5)	3647.6(4)
Z	2	4
F(000)	1332.0	1912.0
2θ range for data collection (deg)	5.654–147.304	8.262–152.526
Final R1[a], wR_2[b]	0.0432, 0.1130	0.1022, 0.1832
Goodness-of-fit on F^2	1.036	1.027

$w = 1 / [\sigma^2(F_o)^2 + 0.0297\ P^2 + 27.5680P]$, where $P = (F_o^2 + 2\ F_c^2) / 3$.
[a] $R_1 = \Sigma||F_o|-|F_c||\Sigma\ /\ |F_o|$.
[b] $wR_2 = [\Sigma w(F_o^2 - F_c^2)^2\ /\ \Sigma w(F_o^2)^2]^{1/2}$.

Table 2
Selected bond lengths (Å) and angles (°) for complexes **1** and **2**.

Complex 1			
Cu(1)-O(6)	2.407(4)	Cu(4)-O(2)	1.966(4)
Cu(1)-O(9)	2.367(4)	Cu(4)-O(3)	2.306(4)
Cu(1)-O(7)	1.995(4)	Cu(4)-O(1)	1.944(4)
Cu(1)-O(8)	2.018(4)	Cu(4)-N(2)	1.985(5)
Cu(1)-N(5)	1.998(5)	Cu(4)-N(1)	2.015(4)
Cu(1)-N(4)	2.006(5)		
O(9)-Cu(1)-O(6)	164.58(13)	N(4)-Cu(1)-O(9)	97.30(16)
O(7)-Cu(1)-O(6)	85.14(14)	N(4)-Cu(1)-O(8)	176.39(18)
O(7)-Cu(1)-O(9)	84.84(15)	O(2)-Cu(4)-O(3)	90.65(14)
O(7)-Cu(1)-O(8)	95.17(16)	O(2)-Cu(4)-N(2)	93.32(18)
O(7)-Cu(1)-N(5)	176.91(17)	O(2)-Cu(4)-N(1)	173.28(18)
O(7)-Cu(1)-N(4)	88.43(18)	O(1)-Cu(4)-O(2)	93.66(17)
O(8)-Cu(1)-O(6)	85.84(14)	O(1)-Cu(4)-O(3)	91.29(16)
O(8)-Cu(1)-O(9)	83.42(14)	O(1)-Cu(4)-N(2)	172.18(18)
N(5)-Cu(1)-O(6)	94.30(15)	O(1)-Cu(4)-N(1)	92.13(18)
N(5)-Cu(1)-O(9)	96.31(15)	N(2)-Cu(4)-O(3)	92.14(16)
N(5)-Cu(1)-O(8)	87.82(17)	N(2)-Cu(4)-N(1)	80.70(18)
N(5)-Cu(1)-N(4)	88.58(18)	N(1)-Cu(4)-O(3)	92.61(15)
N(4)-Cu(1)-O(6)	94.11(16)		

Complex 2			
Co(1)-O(4)	2.124(4)	Co(1)-N(2)	2.114(4)
Co(1)-O(6)	2.207(4)	Co(1)- O(3)	2.058(5)
Co(1)-N1	2.153(4)	Co(1)-N(4) #1	2.090(4)
O(4)-Co(1)-O(6)	59.74(13)	O(3)-Co(1)-N(1)	103.66(19)
O(4)-Co(1)-N(1)	167.20(15)	O(3)-Co(1)-N(2)	163.00(19)
N(1)-Co(1)-O(6)	109.75(15)	O(3)-Co(1)-N(4)#1	97.60(19)
N(2)-Co(1)-O(4)	93.63(15)	N(4)#1-Co(1)-O(4)	98.53(15)
N(2)-Co(1)-O(6)	84.86(15)	N(4)#1-Co(1)-O(6)	158.20(15)
N(2)-Co(1)-N(1)	77.45(15)	N(4)#1-Co(1)-N(1)	92.03(16)
O(3)-Co(1)-O(4)	82.19(18)	N(4)#1-Co(1)-N(2)	99.32(16)
O(3)-Co(1)-O(6)	78.79(17)		

Symmetry transformations used to generate equivalent atoms: #1–1/2 + X, −1/2 + Y, +Z for **2**.

2.5. Stability determination

Having a good stability of the complexes is a prerequisite for further biological studies, and it was evaluated in saline **[29]**. Complexes are soluble at 4×10^{-5} M in Tris-HCl/NaCl buffer (10 mM Tris-HCl/50 mM NaCl, pH 7.40) containing 0.5% dimethylsulfoxide (DMSO). This study set up a series of different period times (10 min, 1 h, 24 h, 48 h and

72 h) respectively. Then, UV–vis absorption spectra was recorded with a Specord 200 UV–visible spectrophotometer.

2.6. DNA binding experiments

DNA stability studies and DNA binding studies include ethidium bromide exchange and CD assay were conducted according to the procedure reported by us previously [30].

2.7. Molecular docking studies

The docking studies of the complexes with DNA duplex of sequence d(5′-G-Diu-TGCAAC-3′) (PDB ID: 454D) were performed using AutoDock 4.2 program. The X-ray crystal structure of the complex was converted into PDB format using Mercury software. The molecular structures optimization of the complexes were completed on the Gaussian09 using the M06 method. After the molecular docking, the output was further analyzed using PyMOL software.

2.8. DNA cleavage experiments

DNA cleavage experiments were assessed by agarose gel electrophoresis with pBR322 plasmid DNA in Tris-HCl/NaCl buffer. The reaction solution was prepared by mixing 5 μL varying concentrations of complexes **1** (10–100 μM), 1 μL pBR322 DNA, 0.1 mM ascorbate (Asc) and it was used only for complex **1**, in which 50 mM Tris–HCl/50 mM NaCl solution were made up to a final volume of 10 μL. After incubation at 37 °C for 2 h, the samples should run electrophoresis on a 1% agarose gel in Tris/acetic acid/EDTA buffer for 70 min at 80 V. The gel image could be obtained by Gel Imaging System (Thmorgan, Beijing, China) after staining for 7 min with EB solution.

To identify the cleavage mechanism of complex **1**, typical ROS scavengers such as dimethyl sulfoxide (DMSO), ethanol, potassium iodide (KI), superoxide dismutase enzyme (SOD), and sodium azide (NaN_3) were used to identify whether and which ROS should be responsible for DNA cleavage catalyzed by complex **1**.

2.9. Evaluation of cytotoxicity

The cytotoxicity of complexes **1** and **2** were conducted according to our previous literature, except that human colon cancer cell line (HCT116), human ovarian cancer cell line (Hela), human cholangiocarcinoma cell line (TFK-1) cells were as the tested cell lines, and different concentrations (5–100 μM) of complexes solutions were as the tested concentrations.

2.10. Analysis of cellular uptake

In this research, the TFK-1 cells were treated with different concentrations of complex **1** for 4 h at 37 °C and 5% CO_2. The experiment was performed according to the procedure reported by us previously [30].

2.11. Morphological changes

The cellular and nuclear morphological changes were monitored by Acridine Orange–Ethidium Bromide (AO/EB) and Propidium iodide (PI) according to the protocol previously described [29,31]. In brief, cells were seeded on 6-well plates (3×10^5 cells per well) for 24 h and treated with and without complex **1** solution for 12 h. The cells were washed thrice with phosphate buffered saline (PBS) solution, then stained with an AO and EB mixture (1:1, 10 mM) for 5 min. Similar to AO and EB dual staining, after washed thrice with PBS solution, cells were stained with PI (20 μg/mL) for 15 min. Finally, the samples were observed under an Axiovert 200 M fluorescence microscope (Zeiss, Jena, Germany).

2.12. Induction of apoptosis

TFK-1 cells were seeded in 6-well plates (3×10^5 cells per well) with 10% fetal bovine serum (FBS) supplemented Roswell Park Memorial Institute (RPMI) 1640 culture medium for 24 h. The cells were treated by complex **1** solution for 24 h at 37 °C. Finally, cells were washed and collected, then labeled with the fluorescent dye of Annexin V fluorescein isothiocyanate (Annexin V-FITC) (5 μL) at 37 °C for 30 min in the dark. Whereafter, the dyeing solution of PI (5 μL) was added into each sample to incubate at least for 5 min. Finally, the samples were analyzed with a Guava EasyCyte 6-2I flow cytometer.

2.13. ROS generation

To detect the intracellular ROS generated by complex 1, 3×10^5 TFK-1 cells were plated in each 6 well plate and incubated overnight for attachment. After treatment with complex 1 for 12 h, cells were collected and washed once with PBS, then incubated with 10 μM 2′,7′-dichlorofluorescein diacetate (DCFH-DA) at 37 °C for 20 min. The cells were washed three times with RPMI 1640 and then imaged with fluorescence microscope at 525 nm.

3. Results and discussion

3.1. Crystal structure of $Cu_3(ppbm)_2(SO_4)_3$ (1)

As shown in Fig. 1, crystallographic analysis reveals that trinuclear copper complex **1** crystallizes in triclinic space group *P*-1.

The ORTEP diagram of complex **1** shows that there is a three copper centers in each structure. The asymmetric unit (ASU) consists of two ppbm ligands, three Cu (II) metal centers, three SO_4^{2-} and five H_2O molecules. Three copper metal centers have two different coordination modes, namely, the metal coordinate configuration of the two ends of the copper metal center Cu1, Cu3 of the coordination of the tetragonal pyramid and the middle Cu2 ion formed by the coordination of the configuration of the octahedral geometry. Among them, to form the tetragonal pyramid configuration, Cu1 was coordinated with two N atoms (N1, N2) respectively derived from the ppbm ligand pyridine ring and imidazole ring and three O atoms, with O3 from SO_4^{2-} and another two O atoms (O1w, O2w) from two water molecules. Unlike Cu1, the five coordinate sites of Cu3 were occupied by the N atoms from the ppbm ligand pyridine ring and the imidazole atom on the imidazole ring, the O atoms of the two anionic SO_4^{2-} and a hydroxyl O atom. As shown in Fig. 1, Cu2 was double bridged to Cu1, Cu3 ions by sulfate ion and ppbm ligand. Meanwhile, Cu2 coordinated with N atoms (N4, N5) from the two ppbm ligands and two water molecules (O7w, O8w), exhibiting the octahedral geometry.

Thermogravimetric analysis of air-stable complex 2 (Fig. S2 Supporting information) indicated that the weight loss of 12.57% as temperature was increased from 30 °C to 220 °C is attributable to the loss of disordered solvent molecules, which is in agreement with the endothermic peak near 215.4 °C in the differential scanning calorimetry spectrum. The further decrease **2** was a dinuclear structure, belonging to three triclinic, space group *P*-1. As shown in Fig. 1, each structure had a centrosymmetric dinuclear cobalt complexes, and each asymmetric unit was composed of one ppbm ligands, one Co(II) metal center, two NO_3^-. Co1 metal center was six coordinated with the octahedral geometry configuration, of which the six coordination sites were occupied with one of the N2 atom from the ppbm ligand on and O3 from an anion NO_3^-, taking the vertex position, and two N atoms from two ppbm ligands (N1, N4a) and two O atoms from another anion NO_3^- (O4, O6), forming a slightly distorted plane.

3.2. Stability analysis

As shown in Fig. 2, complex **1** and **2** were both stable in PBS

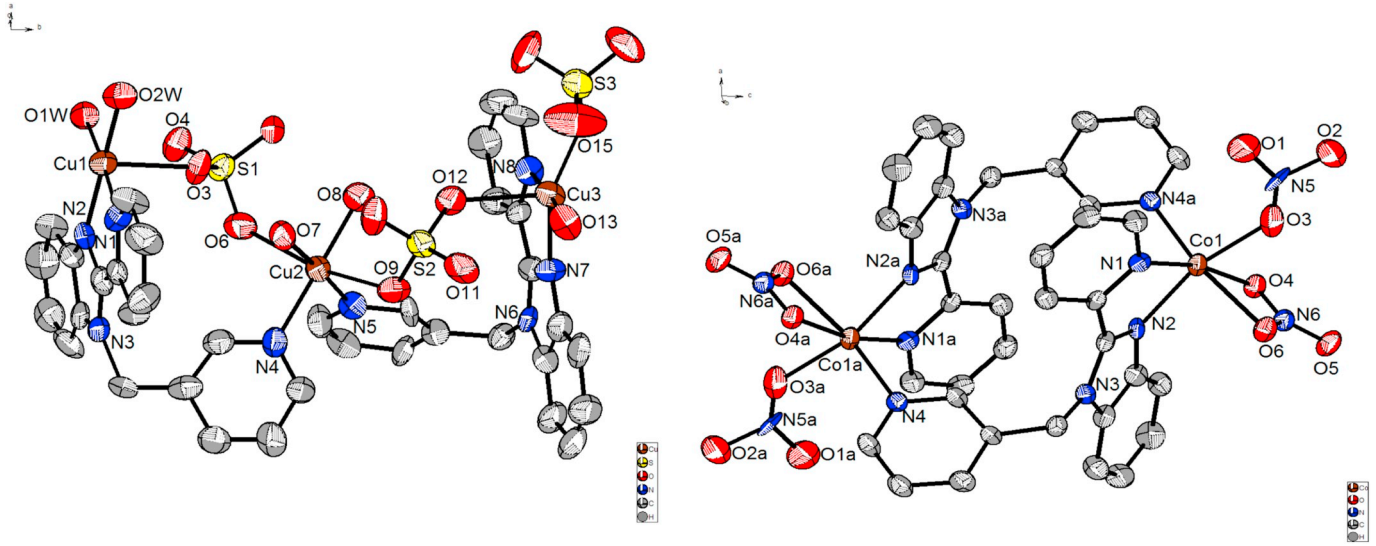

Fig. 1. Crystal structure of $Cu_3(ppbm)_2(SO_4)_3$ (**1**) and $Co_2(ppbm)_2(NO_3)_4$ (**2**).

solution as measured by UV-VIS for 72 h, except that both of complexes displayed hypochromicity since changing their effective concentration for UV–vis absorption, indicating its stability under physiological conditions.

3.3. DNA binding studies

3.3.1. Ethidium bromide exchange

Usually EB emits fluorescence in the presence of DNA due to its strong intercalation between the adjacent DNA base pairs, and when EB is displaced, the fluorescence emission will be decrease **[33]**. Hence, competitive binding experiments were carried out to further determine the DNA binding behavior of the complexes **1** and **2**. As shown in Fig. 3, a dramatic fluorescence quenching can be easily observed as the titration of the complex **1** solution at 608 nm and a red shift of 8 nm (λ_{max} 608 → 617 nm) due to the decreasing π–π* transition energy, suggesting the EB molecules were replaced by **1** under investigation. Similarly, complex **2** also showed a significant fluorescence quenching at λ_{max} = 608 nm with the increment of the complex **2**. To quantitatively assess the quenching efficiency of the different complexes with CT-DNA, we evaluated the above data using the Stern–Volmer equation:

$$F^0/F = 1 + K_{SV}[complex]$$

wherein F^0 and F are the emission intensities in the absence and the presence of the complex, respectively; [complex] is the concentration of complex; K_{sv} is the Stern–Volmer dynamic quenching constant. The K_{sv} values of the complexes **1** and **2** obtained via the plot of F^0/F vs. [complex] are 1.7×10^4 and 2.2×10^3, respectively. The apparent binding constant (K_{app}) is obtained by the equation: K_{EB} [EB] = K_{app} [complex], and the complex concentration was the value at a 50% reduction of fluorescence intensity of EB. The K_{app} value is estimated as $3.4 \times 10^6\ M^{-1}$, and $4.4 \times 10^5\ M^{-1}$, It was clear from the data that the two complexes could efficiently expel out EB, suggesting they might interact with DNA in a strong interaction mode, and complex **1** bound more tightly with DNA than complex **2**.

3.3.2. CD assay analysis

Circular dichroism (CD) is used to monitor the potential DNA conformational changes when the DNA interacts with the metal complex in solution. It has been reported that the characteristic of B-DNA show a positive band at 275 nm caused by base stacking and a negative band at 245 nm caused by helicity, which is sensitive to figure out the bind modes between the complex and DNA **[34]**. As show in the Fig. 4, the intensity of the positive bands of the CD spectra of CT-DNA was decreased significantly upon addition of the complex **1** solution, accompanied with an obvious red shift about 7–8 nm only for the positive

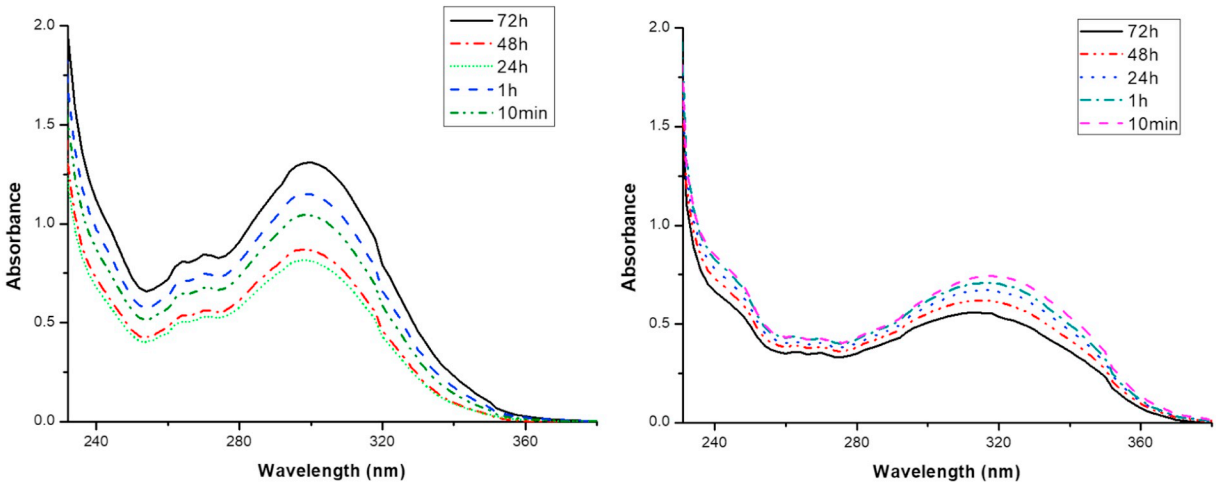

Fig. 2. Absorption spectra of complex **1** and **2** in 0.5% DMSO-Tris-HCl/NaCl buffer (25 °C) at different time points.

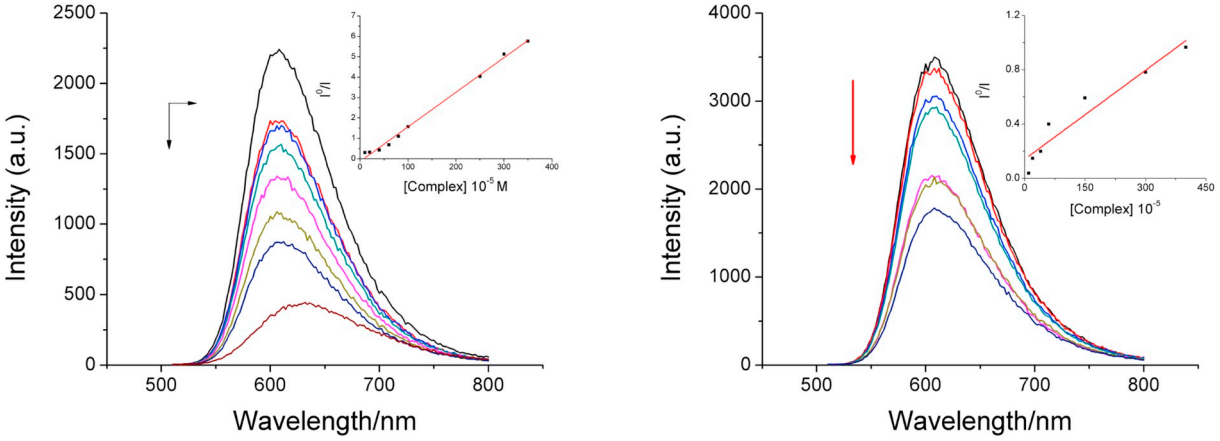

Fig. 3. The results of the fluorescence ethidium bromide (EB) displacement titration assay showing the fluorescence quenching of the EB–DNA system upon the addition of complex **1** and **2**.

band, and nearly no change can be found in negative band, which showed a clear indication that the complexes interacted with DNA thereby disturbed the base stacking involving a stacking interaction between the benzimidazole heteroaromatic plane of the complexes and the adjacent base pairs of DNA and without the ability to unwind the DNA helix resulting in the loss of helicity. However, the CD spectra of CT-DNA treated with the complex **2** resulted in a slight perturbation in the positive band and no change observed in the negative band. Combined with previous experiment, an intercalative binding mode likely due to a strong stacking interaction between the extended planar aromatic phenyl of the two complexes and the DNA base pairs can be concluded, complex **1** behaved a more potent interaction with DNA than complex **2**.

3.4. Molecular docking analysis

Docking technique is a useful technique to visualize the interactions between complexes and DNA for the rational drug design [35]. As the energetically most favorable conformation of the docked pose were shown in Fig. 5, both the complexes were inserted into the empty cavity within GC/GC base pairs rich region from the DNA central position. Thus, the hydrophobic interaction was the major force. The binding energy for complex 1 and 2 with DNA was -9.7 and -8.2 kcal mol^{-1}, which is consistent with the above experimental results.

3.5. DNA cleavage experiments

DNA is one of the most imperative cellular targets for complexes to exhibit good anticancer activity [36,37]. The DNA endonucleolytic cleavage is a common and preliminary method to assess the effect caused by the complex to DNA. As has been proved by above experiments, **1** has more potent affinity to DNA than **2**, it is essential to further evaluate its cleavage activity. The results are shown in Fig. 6, in which the amount of Form I DNA was gradually diminished with the increasing concentration of complex **1** in the presence of ascorbate, correspondingly, the nicked form of DNA (Form II) with single-strand breaks significantly increased. The result indicated that the complex **1** behaves as a strong chemical nuclease compared to that enzymic nucleases.

In addition, it is reported that the radical production mediated by transition metal ions is in charge of catalyzing the DNA cleavage [38]. And it is known that the cleavage mechanism could be attributed to oxidative or hydrolytic pathway [2]. In general, a major cause of DNA damage is the generation of ROS during the interaction between the metal complex and DNA [39]. Hence, The preliminary mechanism of pBR322 DNA cleavage by **1** performed by addition of a variety of radical scavengers including KI, SOD, DMSO, NaN_3 and EDTA. The results showed that cleavage activity decreased apparently in the presence of KI (lane 4) and EDTA (lane 8) (Fig. 7), which is indicative of the involvement of hydrogen peroxide and complexation of benzimidazole with the Cu^{2+} iron in the DNA scission process. Nevertheless, no obvious inhibitions were observed in the presence of NaN_3 and DMSO (lane 6 and lane 7). These results could rule out the possibility of DNA cleavage by the hydroxyl and singlet oxygen radicals. On the other hand, the vitamin C and SOD assist the DNA cleavage activity of **1**. From these results we concluded that complex **1** was capable of

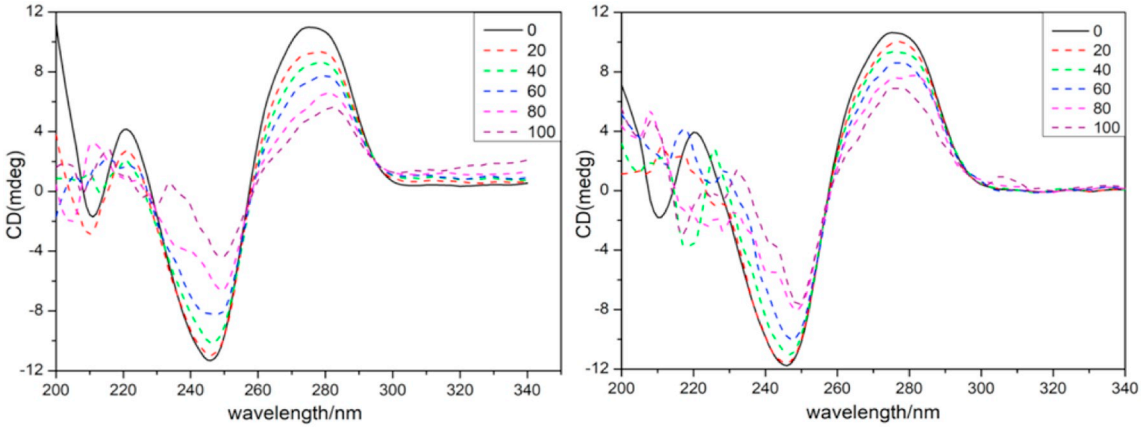

Fig. 4. The CD spectra of complexes **1** and **2** (0–100 μM) upon the titration of CT-DNA in Tris-HCl buffer.

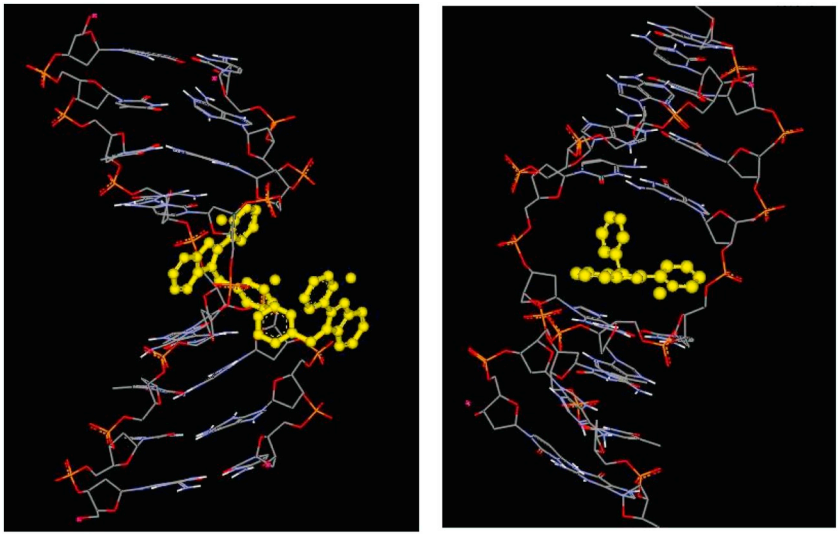

Fig. 5. Molecular docked models of complexes 1 (left) and 2 (right) with DNA.

promoting DNA cleavage through an oxidative DNA damage pathway, and generated copper-oxido species by the reaction of copper and endogenous dioxygen to give hydrogen peroxide.

3.6. Cytotoxicity analysis

The results obtained from the DNA interaction studies for complexes **1** and **2** have encouraged us to test their anticancer properties against cancer cells. With the calculated IC_{50} results as shown in Table 3, complexes **1** and **2** showed a strong inhibitory effect on these three cells with a time and dose dependent effects. The IC_{50} of complex **1** was much lower than that of complex **2** on the whole, which indicated that the inhibitory effect of complex **1** on these three cells was generally better than that of complex **2**. The IC_{50} of complex **1** at 48 h against Hela, HCT116 and TFK-1 cells were 38.0 ± 0.5 μM, 30.3 ± 1.5 μM and 14.7 ± 0.6 μM, respectively (Fig. 8). And the cytotoxicity on TFK-1 cells was stonger than that of cisplatin (17.5 ± 1.89 M) and significantly stronger than the ligand and corresponding metal salts. The results showed that the complexes **1** and **2** had good antitumor effect, and the inhibition effect of complex **1** was more prominent, which confirmed that the copper complexes were specifically active on cancer cells.

3.7. Cellular uptake properties

The cytotoxicity of complex was considered to be positively related to its cellular uptake **[40]**. TFK-1 cells (30×10^4/well) in 6 well plate were exposed to 0, 10 and 20 μM Cu(II) complex solution for 4 h, and the result was reported as ng of copper per 10^6 cell number. As shown in the Fig. 9, the uptake levels were reached 8.17 ± 0.09 and 8.57 ± 0.18 ng/10^6 cells respectively for the concentrations of **1** solution for 10 and 20 μM after 4 h treatment, and the intracellular dose increased about 158% and 172% compared to the dose in untreated control cells, which were also much higher than the dose in the mitochondrion and the cytoplasm. The result suggested that the copper complex prefer to accumulate within nucleus, which was consistent with its cytotoxicity performed by MTT assay and DNA damage-inducing effects.

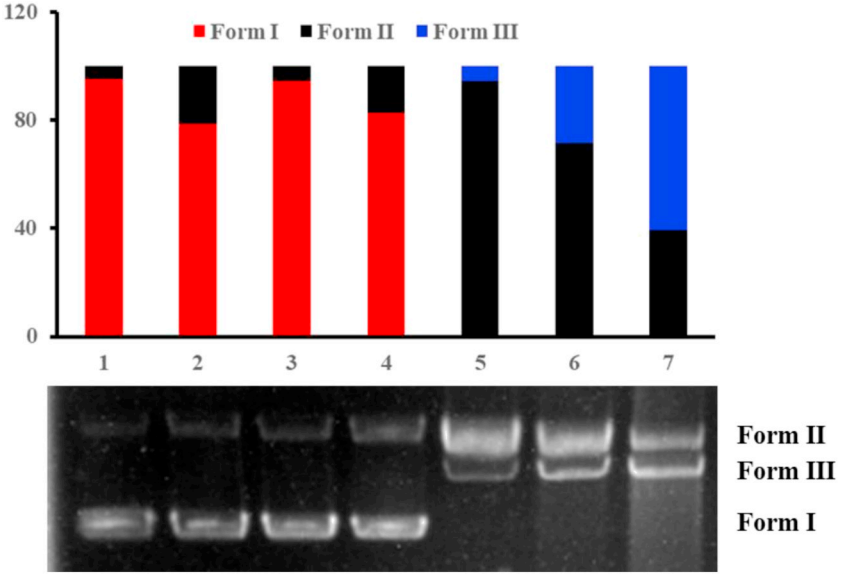

Fig. 6. The cleavage patterns of the agarose gel electrophoresis and corresponding cleavage extent for pBR322 plasmid DNA. Lane 1, DNA; Lane 2, DNA + 1(100 μM); Lane 3, DNA + Asc; lane 4–7, DNA + Asc + 1 (10, 40, 80, 100 μM, respectively).

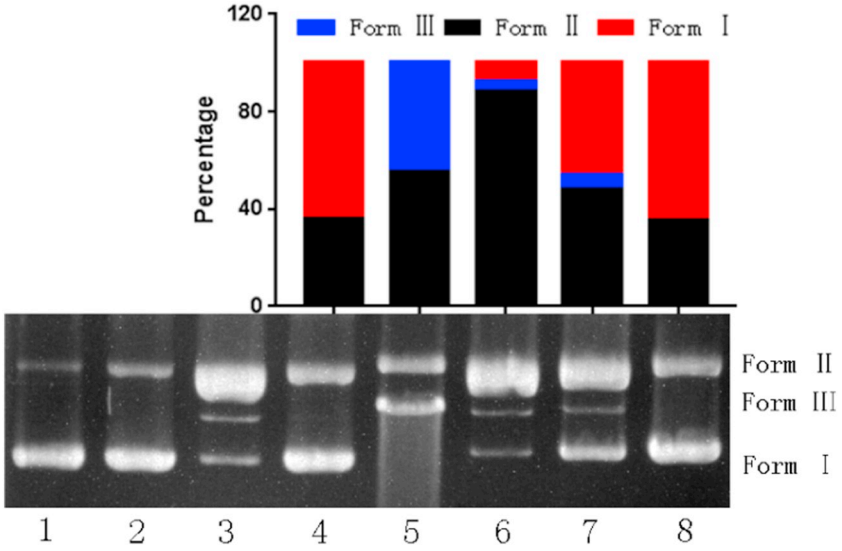

Fig. 7. Agarose gel electrophoresis patterns for the cleavage of pBR322 DNA by **1** in the presence of different typical reactive oxygen species scavengers at 37 °C after 3 h of incubation. (a) Lane 1, DNA; lane 2, DNA + 1 (50 mM); lane 3, DNA + 1 (50 mM) + Asc (1 mM); lane 4, DNA + Asc (1 mM) + KI (1 mM) + 1 (50 mM);lane 5, DNA + Asc (1 mM) + SOD (30 units) + 1 (50 mM);lane 6, DNA + Asc (1 mM) + NaN3 (1 mM) + 1 (50 mM); lane 7, DNA + Asc (1 mM) + DMSO (1 mM) + 1 (50 mM); lane 8, DNA + Asc (1 mM) + EDTA (1 mM) + 1 (50 mM).

Table 3
Cytotoxicity of the two complexes in three cancer cell lines.

IC_{50} (μM)						
	Complex 1			Complex 2		
	24 h	48 h	72 h	24 h	48 h	72 h
Hela	56.10 ± 1.71	38.00 ± 0.53	18.90 ± 0.72	78.20 ± 2.53	39.40 ± 2.19	39.00 ± 2.04
HCT116	69.70 ± 2.33	30.30 ± 1.49	25.10 ± 1.60	116.90 ± 1.10	34.60 ± 1.51	25.50 ± 5.49
TFK-1	20.10 ± 1.41	14.70 ± 0.56	0.70 ± 0.87	> 100	67.70 ± 1.34	55.40 ± 1.00

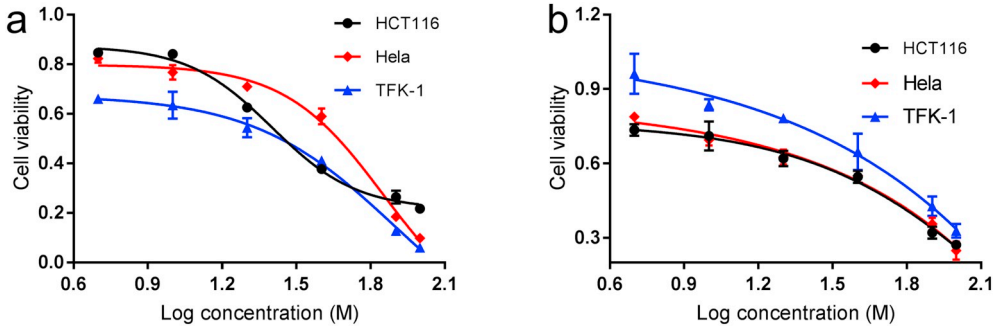

Fig. 8. Inhibition curve showing inhibition rate verses drug concentration (mmol/L) against HCT116, Hela, TFK-1 cell lines for48 h Inhibition curve for complex 1 1(a); Inhibition curve for complex 2 (b).

3.8. Induction of apoptosis

Acridine Orange–Ethidium Bromide (AO/EB) staining experiment were employed to determine the mode of cell death via visualizing the morphology of the cells and nucleus with the complex **1** solution in TFK-1 cells. AO, a fluorescent dye, stains the DNA of live cells and dead cells, and EB is used to stain the DNA of dead cells that have lost membrane integrity. After the treatment by AO/EB dual staining, apoptotic cells always show reddish-orange, necrotic cells with red fluorescence, and the living cells always show a uniform level of green [41]. As shown in the upper of Fig. 10, a clearly and uniform green can be observed in the control cells. Correspondingly, an increasing number of treated cells are reddish-orange upon the complex **1** concentration increment (30 μM, 40 μM).

Propidium iodide (PI), which is a well-known fluorescent staining dye for nucleus, was used to visualize the nuclear morphological changes in the treated TFK-1 cells by 1.16. The samples were prepared similarily to the AO/EB staining. The control group exhibited an evenly stained contours of the nuclei, whereas the treated cell groups were companied with typical characteristics of apoptosis, such as, fragmented, highly condensed nuclei and membrane blebbing. Thus the results suggested that the mode of cell death was apoptosis induced by the complex **1**.

Then, phosphatidylserine externalization represented the occurrence of apoptosis in the early stage of apoptosis [42]. Hence, the Annexin V-FITC Apoptosis Detection Kit—was employed to further determine the ability of complex **1** to induce apoptosis. At the onset of cell apoptosis, the phosphatidylserine will be transfer to the outer side of the cell membrane, which can be detected by the annexin-V protein in the presence of calcium(II) ions, while that can be stained with PI once the cells are necrosis [43]. The results were shown in the bottom of Fig. 9, compared to the control cells which have no apoptosis and necrotic features, the complex **1** induced a huge late apoptosis in 7.10% and 31.84% of TFK-1 cells at the concentration of 30 μM and 40 μM

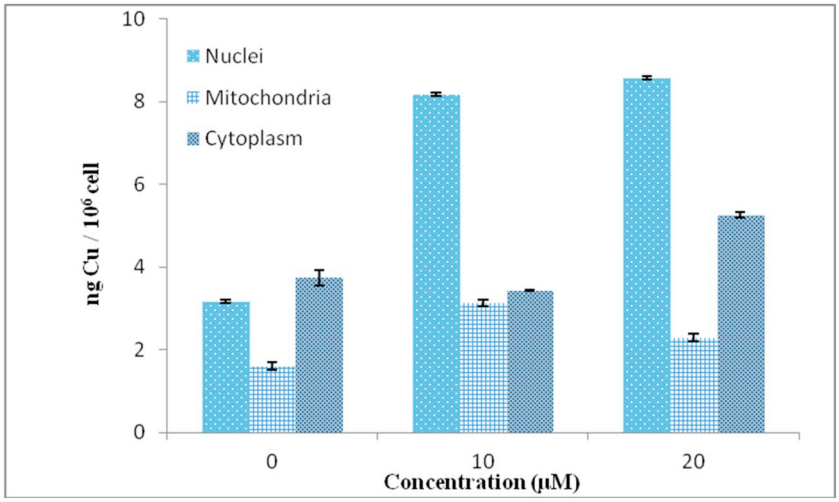

Fig. 9. ICP-MS assay for complex **1** distributed in the cell nucleus and cytoplasm with different concentrations.

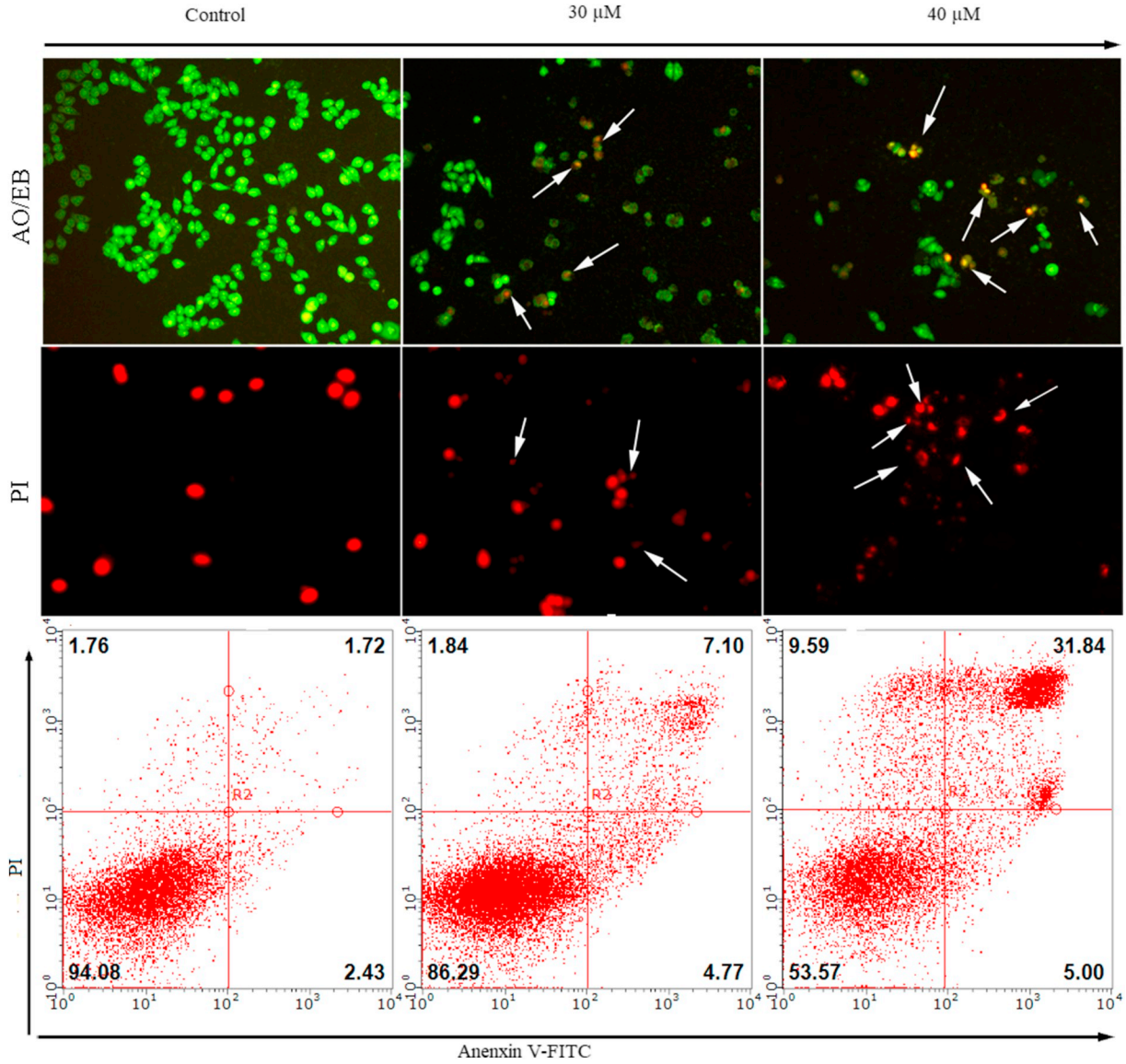

Fig. 10. Apoptosis determination. The upper: Morphological changes of TFK-1 cells treated with various concentration of 1 for 48 h which were double stained with AO/EB and detected by fluorescence microscope. The middle: Morphological changes of TFK-1 cells treated with various concentration of 1 for 48 h which were double stained with PI. The bottom: the induce apoptosis by labeling with Annexin V-FITC and PI.

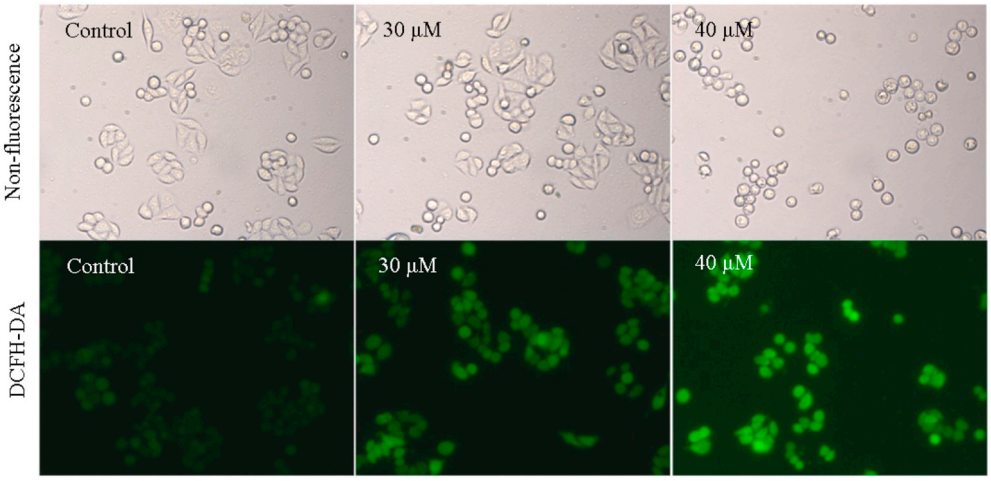

Fig. 11. ROS detection by labeling with DCFH-DA and detected by fluorescence microscope.

respectively, accompanied with a slight early apoptosis. These results collectively indicate that **1** induces cell death mainly through apoptosis.

3.9. Elevation of ROS

Have learned that **1** can efficiently induce cell apoptosis, Next we analyzed the molecular mechanism of apoptosis involved in this process. The level of reactive oxygen species (ROS) intracellular in apoptotic cells can be overexpressed and it closely relates to the cellular uptake of metal complexes and the induction of mitochondrial dysfunction **[44]**. A DCFH-DA assay was used to measure ROS in TFK-1 cells produced by treatment of complex **1**, DCFH-DA itself does not have fluorescence, which is able to generate non-blooming DCFH by the process of intracellular esterase, and DCFH can easily oxidized to fluorescent DCF by ROS **[45]**. The green fluorescence intensity ascribes to the level of ROS. As shown in Fig. 11, after treatment by the complex **1** with TFK-1 cells, in contrast to the control cells with no fluorescence observed, the treated cells exhibit an increasing fluorescence with the added concentration of the complex **1**. The result infers complex **1** could generate ROS to induce apoptosis in TFK-1 cells, which is consistant with the results obtained from DNA cleavage experiment. Usually the higher levels of ROS is induced by copper-redox species to induce oxidative DNA damage and cell death **[46,47]**.

4. Conclusions

In conclusion, this paper reported the synthesis and structural characterization of two complexes, $Cu_3(ppbm)_2(SO_4)_3$ (**1**) and $Co_2(ppbm)_2(NO_3)_4$ (**2**). The trinuclear complex **1** exhibited a moderate binding ability with DNA via intercalation mode. The new complexes were screened for cytotoxic activity against HCT116, Hela, TFK-1 cancer cell lines, and they were found to exhibit good cytotoxicity to cancer cells. The activity of complex **1** was significantly superior to that of cisplatin and **2**. Complex **1** was shown to accumulate preferentially in nucleus in the TFK-1 cells and induced apoptosis which involved ROS generation. And further mechanism analysis demonstrated that **1** rendered elevated cellular ROS levels by generating hydrogen peroxide via gel electrophoresis, thereby efficiently cleaving DNA at a low efficient concentration. Thus, the complex **1** has the potential to be developed as a chemotherapeutic agent for the treatment of cancer diseases. The data from our present study suggested that **1** deserves detailed antitumor mechanistic further investigation as new antitumor drugs.

Crystallographic data for complexes **1** and **2** have been deposited with the Cambridge Crystallographic Data Centre < 1873013–1873014 > . These data can be freely accessed at www.ccdc.cam.ac.uk/conts/retrieving.html, or obtained from the Cambridge Crystallographic Data Centre, 12 Union Road, Cambridge CB2 1EZ, UK (fax: +44 1223-336-033). Supplementary data to this article can be found online at doi:https://doi.org/10.1016/j.jinorgbio.2019.110696.

Acknowledgment

This study was supported by the National Natural Science Foundation of China (Nos. 21371046, 21401041).

References

[1] T.W. Hambley, Dalton Trans. (2007) 4929.
[2] F. Arnesano, G. Natile, Coord. Chem. Rev. 253 (2009) 2070.
[3] M. Pellei, G.G. Lobbia, C. Santini, R. Spagna, M. Camalli, D. Fedeli, G. Falcioni, Dalton Trans. (2004) 2822.
[4] C. Santini, M. Pellei, G.G. Lobbia, S. Alidori, M. Berrettini, D. Fedeli, Inorg. Chim. Acta 357 (2004) 3549.
[5] X.Y. Wang, Z. Guo, J. chem.soc.Rev. 42 (2013) 202–204.
[6] N. Muhammad, Z.J. Guo, Curr. Opin. Chem. Biol. 19 (2014) 144 – 153.
[7] Barry, N. P. E.; Sadler, P. J. Exploration of the medical periodic table: towards new targets. Chem. Commun. 2013, 49, 5106–5131.
[8] A. Oleksi, A.G. Blanco, R. Boer, I. Uson, J. Aymami, A. Rodger, M.J. Hannon, M. Coll, Angew. Chem. Int. Ed. 45 (2006) 1227 – 1231.
[9] P. Wang, C.H. Leung, D.L. Ma, R.W.Y. Sun, S.C. Yan, Q.S. Chen, C.M. Che, Angew. Chem. Int. Ed. 50 (2011) 2554 – 2558.
[10] D.L. Ma, H.Z. He, K.H. Leung, D.S.H. Chan, C.H. Leung, Bioactive luminescent transition-metal complexes for biomedical applications, Angew. Chem. Int. Ed. 52 (2013) 7666 – 7682.
[11] Bergamo, A.; Sava, G. Ruthenium anticancer compounds: myths and realities of the emerging metal-based drugs. Dalton Trans.. 2011, 40, 7817–7823.
[12] T.Y. Han, T.S. Guan, M.A. Iqbal, R.A. Haque, K. Sharmila Rajeswari, M.B. Khadeer Ahamed, A.M.S. Abdul Majid, Med. Chem. Res. 23 (2013) 2347–2359.
[13] C. Marzano, M. Pellei, F. Tisato, C. Santini, Anti Cancer Agents Med. Chem. 9 (2009) 185–211.
[14] D. Palanimuthu, S.V. Shinde, K. Somasundaramand, A.G. Samuelson, J. Med. Chem. 56 (2013) 722 – 734.
[15] S. Tardito, A. Barilli, I. Bassanetti, M. Tegoni, O. Bussolati, R. Franchi-Gazzola, C. Mucchinoand, L. Marchiò, J. Med. Chem., 2012, 55, 10448 – 10459.
[16] F. Tisato, C. Marzano, M. Porcbia, M. Pellei, C. Santini, Med. 17Res. Rev. 30 (2010) 708 – 749.
[17] S. Zeno, M. Zaaroor, S. Leschiner, L. Veenman, M. Gavish, Biochem 48 (21) (2009) 4652–4661.
[18] G.K. Harris, X. Shi, Mutat. Res. 533 (2003) 183–200.
[19] M.T. Santore, D.S. McClintock, V.Y. Lee, G.R. Budinger, N.S. Chandel, Am. J. Phys. 282 (2002) 727–734.
[20] E. Griguer, C. Oliva, E. Kelley, G. Giles, J. Lancaster, G. Gillespie, Cancer Res. 66 (2006) 2257–2263.
[21] D.R. Green, J.C. Reed, Science 281 (1998) 1309–1312.
[22] M. Chen, et al., Dalton Trans. 44 (29) (2015) 13369–13377.
[23] X.B. Fu, J.J. Zhang, D.D. Liu, Q. Gan, H.W. Gao, Z.W. Mao, X.Y. Le, J. Inorg. Biochem. 143 (2015) 77–87.
[25] X. Meng, L. Liu, H. Zhang, Y. Luo, C. Liu, Dalton Trans. 40 (2011) 12846–12855.
[26] N. Selvakumaran, N.S. Bhuvanesh, R. Karvembu, Dalton Trans. 43 (2014) 16395–16410.
[27] M. Mohamed Subarkhan, R.N. Prabhu, R. Raj Kumar, R. Ramesh, RSC Adv. 6 (2016) 25082–25093.

[28] Imtiyaz Yousuf, Farukh Arjmand, Sartaj Tabassum, Loic Toupet, Rais Ahmad Khanc and Maqsood Ahmad Siddiqui, Dalton Trans.. 44(2015) 10330–10342.
[29] J.A. Zhao, H.B. Yu, S.C. Zhi, R.N. Mao, J.Y. Hu, X.X. Wang, Chinese. Chem. Lett. 28 (2017) 1539–1546.
[30] B. Deka, T. Sarkar, S. Banerjee, A. Kumar, S. Mukherjee, S. Deka, K.K. Saikia, A. Hussain, Dalton Trans. 46 (2017) 396–409.
[31] A.Q. Ali, S.G. Teoh, N.E. Eltayeb, M.B. Khadeer Ahamed, A.M.S. Abdul Majid, Polyhedron 74 (2014) 6–15.
[33] N. Shahabadi, M. Pourfoulad, A. Taherpour, J. Coord. Chem. 70 (2017) 201–222.
[34] R. Rohs, I. Bloch, H. Sklenar, Z. Nucl Shakked, Acids Res 33 (2005) 7048–7057.
[35] P. Govender, A.K. Renfrew, C.M. Clavel, P.J. Dyson, B. Therrien, G.S. Smith, Dalton Trans. 40 (2011) 1158 – 1167.
[36] Liu, H. K.; Berners-Price, S. J.; Wang, F. Y.; Parkinson, J. A.; Xu, J. J.; Bella, J.; Sadler, P. J. 2010 , 118 (48) :8333–8336.
[37] T. Afrati, A.A. Pantazaki, C. Dendrinou-Samara, C. Raptopoulou, A. Terzis, D.P. Kessissoglou, Dalton Trans. 39 (2010) 765–775.
[38] B. Barut, A. Sofuoglu, Z. Biyiklioglu, A. Ozel, Dalton Trans. 45 (2016) 14301–14310.
[39] L.M. Chen, F. Peng, G.D. Li, X.M. Jie, K.R. Cai, C. Cai, Y. Zhong, H. Zeng, W. Li, Z. Zhang, J.C. Chen, J. Inorg. Biochem. 156 (2016) 64–74.
[40] A. Paul, S. Anbu, G. Sharma, M.L. Kuznetsov, B. Koch, M.F. Guedes da Silva, A.J. Pombeiro, Dalton Trans. 44 (2015) 19983–19996.
[41] C. Tan, S. Wu, S. Lai, M. Wang, Y. Chen, L. Zhou, Y. Zhu, W. Lian, W. Peng, L. Ji, A. Xu, Dalton Trans. 40 (34) (2011) 8611–8621.
[42] P. Raj, A. Singh, A. Singh, N. Singh, Dalton Trans. 46 (3) (2016) 985.
[43] G. Gasser, I. Ott, N. Metzlernolte, J. Med. Chem. 54 (2011) 3–25.
[44] S. Bittner, T. Ruck, M.K. Schuhmann, A.M. Herrmann, H.M.O. Maati, N. Bobak, K. Goebel, F. Langhauser, D. Stegner, P. Ehling, M. Borsotto, H.-C. Pape, B. Nieswandt, C. Kleinschnitz, C. Heurteaux, H.-J. Galla, T. Budde, H. Wiendl, S.G. Meuth, Nat. Med. 19 (9) (2013) 1161 – 1165.
[45] T.B. Thederahn, M.D. Kuwabara, T.A. Larsen, D.S. Sigman, J. Am. Chem. Soc. 111 (1989) 4941–4946.
[46] D.S. Sigman, Acc. Chem. Res. 19 (1986) 180–186.